ACS APPLIED MATERIALS & INTERFACES

Research Article

www.acsami.org

# Gas-Barrier Hybrid Coatings by the Assembly of Novel Poly(vinyl alcohol) and Reduced Graphene Oxide Layers through Cross-Linking with Zirconium Adducts

Ning Yan,[†,‡] Filomena Capezzuto,[†] Giovanna G. Buonocore,[†] Marino Lavorgna,[*,†] Hesheng Xia,[*,§] and Luigi Ambrosio[†]

[†]Institute of Polymers, Composites and Biomaterials, National Research Council, Piazzalle Fermi, 1-80055 Portici, Naples, Italy

[‡]Xi'an Modern Chemistry Research Institute, Xi'an 710065, China

[§]State Key Laboratory of Polymer Materials Engineering, Polymer Research Institute of Sichuan University, Chengdu 610065, China

Supporting Information

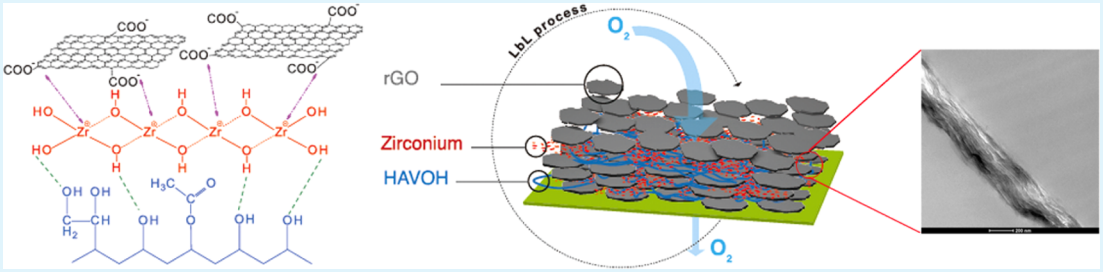


**ABSTRACT:** Gas-barrier materials obtained by coating poly(ethylene terephthalate) (PET) substrates have already been studied in the recent literature. However, because of the benefits of using cheaper, biodegradable, and nonpolar polymers, multilayered hybrid coatings consisting of alternate layers of reduced graphene oxide (rGO) nanosheets and a novel high amorphous vinyl alcohol (HAVOH) with zirconium (Zr) adducts as binders were successfully fabricated through a layer-by-layer (LbL) assembly approach. Atomic force microscopy analysis showed that rGO nanoplatelets were uniformly dispersed over the HAVOH polymer substrate. Scanning and transmission electron microscopies revealed that multilayer $(HAVOH/Zr/rGO)_n$ hybrid coatings exhibited a brick-wall structure with HAVOH and rGO as buildings blocks. It has been shown that 40 layers of HAVOH/Zr/rGO ultrathin films deposited on PET substrates lead to a decrease of 1 order of magnitude of oxygen permeability with respect to the pristine PET substrate. This is attributed to the effect of zirconium polymeric adducts, which enhance the assembling efficiency of rGO and compact the layers, as confirmed by NMR characterization, resulting in a significant increment of the oxygen-transport pathways. Because of their high barrier properties and high flexibility, these films are promising candidates in a variety of applications such as packaging, selective gas films, and protection of flexible electronics.

**KEYWORDS:** *layer-by-layer assembly, reduced graphene oxide, high amorphous poly(vinyl alcohol), polymeric zirconium adducts, barrier properties*

## 1. INTRODUCTION

Graphene (GE) has attracted tremendous interest in the development of multifunctional materials because the single-atom-thick carbon sheet exhibits excellent thermal[1] and electrical conductivity,[2,3] high mechanical strength,[4] and gas-barrier properties. The inclusion of impermeable GE and its derivatives in polymeric materials is widely regarded as a useful approach to meeting the ever-increasing demand of ultrabarrier materials useful in a multiplicity of applications ranging from food to medical sectors and from chemical to electronic fields.[5−7] In order to prepare effective GE-based polymer nanocomposites, it is worth tailoring the GE morphology as uniform GE dispersion, 2D-layered GE-oriented structure, or 3D GE segregated structure, according to the desired final features.[8−10]

Recently, highly ordered GE-based polymer materials with good properties have been fabricated by a variety of methods including solution-casting,[11] spin-coating,[12] vacuum-assisted filtration,[13] and layer-by-layer (LbL) assembly.[14−16] Among those methods, the LbL assembly of cationic and anionic polymers is well-known for its robustness and versatility. The driving force that allows formation of the layered structure is the electronic interaction of polymers with opposite charges. When the anionic polymer is substituted by a graphene oxide (GO) filler, the LbL assembly approach can be used to prepare the hybrid GO/polymer coating, and the structure of the layered coating depends on the pH of the GO suspension,

Received: August 14, 2015
Accepted: September 25, 2015
Published: September 25, 2015





DOI: 10.1021/acsami.5b07529
ACS Appl. Mater. Interfaces 2015, 7, 22678−22685

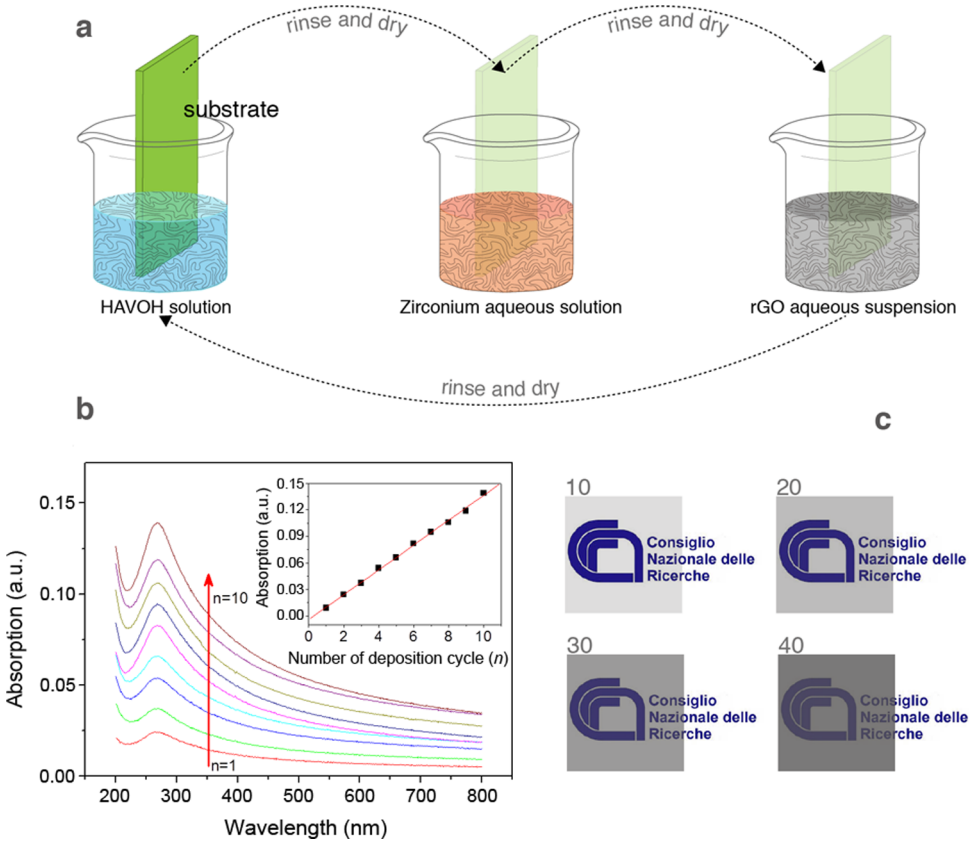


**Figure 1.** (a) Schematic illustration for production of the multilayer organic−inorganic coating deposited on PET substrates by a LbL assembly process. (b) UV−vis absorption spectra of $(HAVOH/Zr/rGO)_n$ (where $n$ = 1, 2, ..., 10 represents the number of deposited HAVOH/Zr/rGO one-layered assemblies) coatings deposited on quartz substrates. Inset: absorbance at 268 nm plotted as a function of the number of deposition cycles. (c) Digital photographs of $(HAVOH/Zr/rGO)_n$ ($n$ = 10, 20, 30, and 40) coatings deposited on PET substrates.

which affects the charge compensation between negatively charged GO nanoplatelets and the positive polymeric counterpart.[17] When the depositing polymers are either nonionic or weakly ionizable, their assembly is promoted by other interactions, such as hydrogen-bonding and covalent bonds.[18−20]

Gas-barrier materials obtained by coating poly(ethylene terephthalate) (PET) substrates with poly(vinyl alcohol) (PVA) or polyethylenimine (PEI) through LbL techniques have already been studied in the recent literatures.[14−16,21−23] Results obtained with PVA-based coatings are not particularly outstanding. On the contrary, PEI-based coatings assembled with GO or montmorillonite exhibit significant enhancement in the barrier properties. However, because of the high cost of a coating solution based on PEI and the benefit of using cheaper, biodegradable, and nonpolar polymers, the use of a novel high amorphous vinyl alcohol (HAVOH) assembled with reduced graphene oxide (rGO) has been proposed in this work. The used HAVOH, patented and commercialized with the trade name of G-Polymer (Nippon-Goshei, Japan), is a new biodegradable polymer based on modified PVA, particularly interesting because of its excellent extrusion processability, ease for coating, and outstanding oxygen barrier properties.

It is worth noting that, in the LbL self-assembly of organic layers, zirconium (Zr)-based compounds have been employed as valuable cross-linkers because of their strong ionizable nature in a water solution and intrinsic capability to promote intermolecular interactions via hydrogen and covalent bonds. The obtained zirconium-based LbL coatings have been used for dielectric devices, electrooptical switching elements, and nonlinear-optical devices.[24−26] However, surprisingly, to the best of our knowledge, zirconium has never been used in the fabrication of multilayered barrier films or coatings. To this aim, in this work we report on the role of an aqueous compound of zirconium(IV) as the cross-linker in LbL deposition of coatings consisting of the novel nonionic HAVOH and low-surface-charge rGO. It has been proven that the zirconium adducts, originating from hydrolysis of oxynitrate $[ZrO(NO_3)_2]$, improve the LbL fabrication and the final properties of the layer assembly composed of HAVOH and rGO on the PET substrate.

## 2. RESULTS AND DISCUSSION

The LbL assembly procedure is schematically illustrated in Figure 1a. The corona-treated PET substrates (23 $\mu$m thick) were initially dipped into the HAVOH aqueous solution (1.0 wt %) for 1 min, then rinsed with deionized water and dried at room temperature, and again dipped into the zirconium(IV) oxynitrate aqueous solution (0.1 wt %) for 30 s. After rinsing and drying, the substrate coated by the layered coating under buildup was finally immersed in a rGO (0.1 mg $mL^{-1}$) aqueous dispersion for 1 min. The hybrid ultrathin coating deposited by the above process is referred to as a one-layered assembly (HAVOH/Zr/rGO). The deposition cycle was repeated until the desired number of layered assemblies was achieved. In order to investigate the effect of zirconium adducts on the gas permeabilities, control samples were prepared by following the same LbL procedure, except for dipping of the substrate into a


DOI: 10.1021/acsami.5b07529
ACS Appl. Mater. Interfaces 2015, 7, 22678−22685

zirconium aqueous solution. Before further characterization, all coated samples were thermally stabilized for 10 min at 120 °C (more details on the experimental procedure and characterization of GO and rGO fillers are presented in the Supporting Information, Figures S1−S3).

UV−vis absorption spectra of $(HAVOH/Zr/rGO)_n$ multilayer films, where $n$ represents the number of layered assemblies HAVOH/Zr/rGO, are shown in Figure 1b. The multilayer films were deposited on quartz substrates, and the spectra were collected after each deposition cycle to monitor the consecutive buildup of the coating during the LbL process. The UV−vis absorption band at 268 nm is ascribed to the assembly of rGO nanosheets. The peak intensity increases linearly with the number of deposited layers (inset graph in Figure 1b), confirming that the LbL deposition is a well-reliable approach. Digital images of PET substrates coated with $(HAVOH/Zr/rGO)_n$ ultrathin coatings (Figure 1c) demonstrate that the prepared coatings are highly homogeneous and that their transparency decreases with an increase in the number of deposited layers.

The $(HAVOH/Zr/rGO)_n$ ultrathin hybrid coatings show a well-defined layered morphology. A scanning electron microscopy (SEM) cross-sectional image of the $(HAVOH/Zr/rGO)_{10}$ hybrid coating deposited on PET substrate is shown in Figure 2a. The coating cross section consisting of distinguishable layers of HAVOH and rGO nanoplatelets has a thickness of about 90 nm in the case of $(HAVOH/Zr/rGO)_{10}$, as was also confirmed by transmission electron microscopy (TEM) analysis (Figure 2b) and grazing-incidence small-angle X-ray scattering (GISAXS) measurements (see Figure S4 in the Supporting Information). The TEM image of the $(HAVOH/Zr/rGO)_{40}$ assembly in Figure 2c shows a coating thickness of about 280 nm corresponding to about a 4-fold thickness of the sample $(HAVOH/Zr/rGO)_{10}$ shown in Figure 2b. This confirms that the thickness of the LbL coating grows almost linearly with the number of layered assemblies. Furthermore, in Figure 2c, the dark lines represent the oriented rGO platelets arranged along PET substrates. They assemble with HAVOH layers assisted by zirconium adducts, thus forming a compact nanobrickwall structure. The surface morphology of the sample coating can be observed in the SEM image of Figure 2d. The rGO platelets, as contoured within the red line, are deposited with their surfaces parallel to the substrates. The rGO capability of covering the surface has been investigated through atomic force microscopy (AFM) analysis. Parts e and f of Figure 2 compare the AFM topographies of one HAVOH/rGO bilayer and a one-layered (HAVOH/Zr/rGO) assembly deposited on the silicon wafer, respectively. In both systems, the rGO nanoplatelets appear as irregular polygonal pieces, with the maximum length size ranging from hundreds of nanometers to a few microns. It is worth noting that the assembly with zirconium exhibits a larger amount of rGO nanoplatelets compared to the sample without zirconium. This is due to specific interactions of zirconium adducts with rGO nanoplatelets, which allow more platelets to be deposited on the HAVOH polymer surface, increasing the surface coverage density. Moreover, the height profiles measured for the two samples (Figure 2e,f) show the presence of rGO platelets embedded in HAVOH polymers, whose heights are difficult to estimate because of the effect of polymer overlapping the GE surface, and appear to be roughly about 6 and 4 nm, respectively, for the sample prepared with and without zirconium adducts.

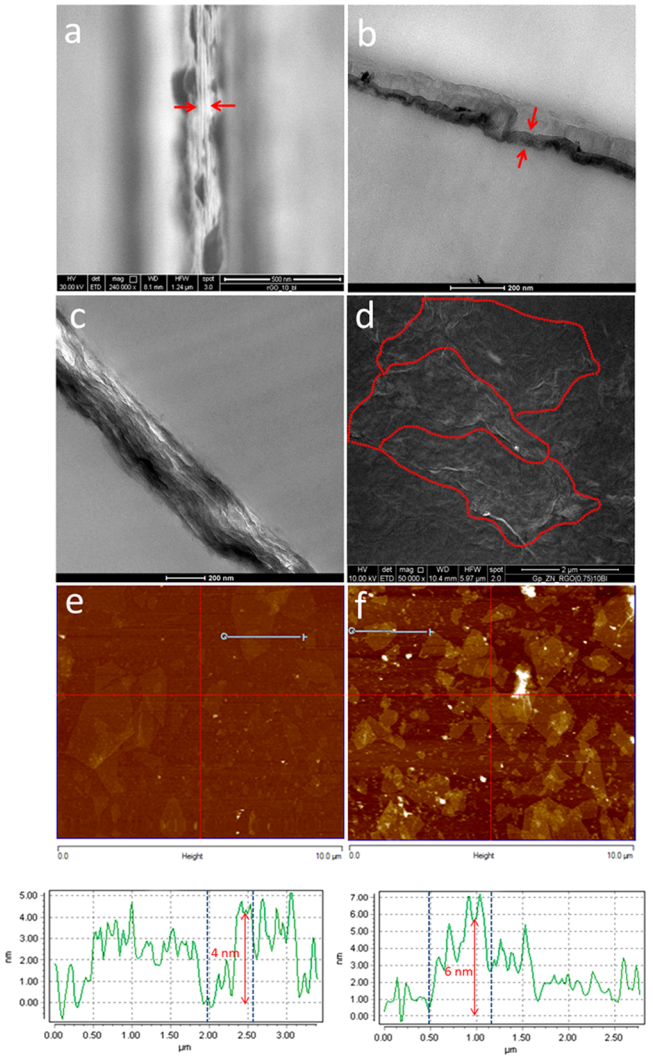


**Figure 2.** Cross-sectional (a) SEM and (b) TEM images of $(HAVOH/Zr/rGO)_{10}$ and (c) $(HAVOH/Zr/rGO)_{40}$ hybrid coatings deposited on PET substrates. The arrow bars highlight the coating thickness. (d) SEM image of the surface of the $(HAVOH/Zr/rGO)_{10}$ coating. The GE platelets are contoured within the dotted line. AFM surface images of (e) $(HAVOH/rGO)_1$ and (f) $(HAVOH/Zr/rGO)_1$ coatings deposited on silicon wafers. Below images (e) and (f) are the corresponding height profiles taken along the gray lines.

The oxygen transmission rates (OTR) of multilayered coatings deposited on PET substrates with and without zirconium adducts were measured at 23 °C and various relative humidity (RH) values (Figure 3). In all of the investigated conditions, the OTRs of coated samples decrease with an increase in the number of deposited assemblies. The OTR values of samples coated with $(HAVOH/rGO)_n$ assemblies without zirconium adducts decrease by about 40% in the case of 40 deposited assemblies (Figure 3d), whereas the OTR values of samples coated with only 10 layers of the HAVOH/Zr/rGO assemblies decrease by about 70% compared with pristine PET in dry conditions, as shown in Figure 3a. With an increase in the number of HAVOH/Zr/rGO assemblies up to 20, 30 and 40, the OTRs of the coated samples further decrease respectively by about 85%, 90%, and 95% with respect to the uncoated PET substrate. The results confirm that the deposition of an increasing number of HAVOH/Zr/rGO assemblies enables the formation of thicker barrier coatings on


DOI: 10.1021/acsami.5b07529
ACS Appl. Mater. Interfaces 2015, 7, 22678−22685

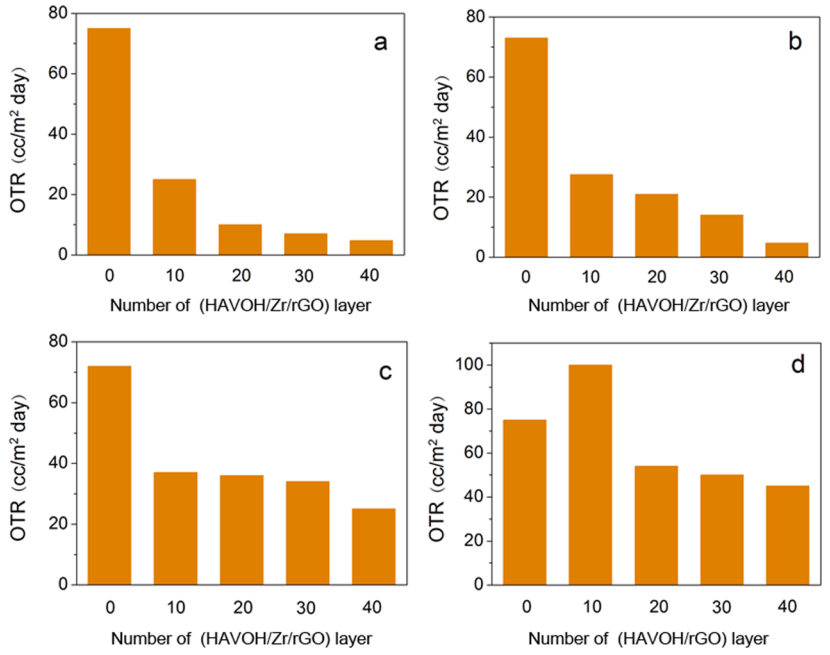


**Figure 3.** OTRs of PET substrates coated with $(HAVOH/Zr/rGO)_n$ multilayered assemblies reported as a function of $n$ (which indicates the number of assemblies). The uncoated PET substrate corresponds to the sample labeled with 0 number of HAVOH/Zr/rGO. Samples were measured at 23 °C and (a) 0%, (b) 33%, and (c) 75% RH. (d) OTRs of a $(HAVOH/rGO)_n$ coating measured at 23 °C and 0% RH. The experimental errors are in the range of 10% of the reported OTR values.

PET substrates, which achieves an extremely tortuous pathway to prevent the permeation of oxygen molecules. The presence of zirconium adducts in the $(HAVOH/Zr/rGO)_n$ hybrid coatings promotes the stronger interactions between rGO nanoplatelets and polymers in the LbL assemblies, as will be discussed in detail below.

Figure 4 shows a comparison of the performances in terms of the permeability and thickness of several LbL coatings realized on PET substrates. The developed $(HAVOH/Zr/rGO)_{40}$ multilayered coating (thickness ≅ 280 nm) has a lower oxygen permeability of $0.014 \times 10^{-20}$ $m^3$ m $m^{-2}$ $s^{-1}$ $Pa^{-1}$ compared to PVA-based coatings obtained through both solvent-casting deposition ($0.003 \times 10^{-20}$ $m^3$ m $m^{-2}$ $s^{-1}$ $Pa^{-1}$, 10 $\mu$m) and the LbL approach ($2.5 \times 10^{-20}$ $m^3$ m $m^{-2}$ $s^{-1}$ $Pa^{-1}$, 40 nm). Data related on a PEI-based coating through the LbL assembly with GO or MMT as fillers are located in the bottom-left side of the diagram, highlighting a better effectiveness in enhancing the barrier properties of multilayer coating assemblies. However, it is worth noting that coating solutions based on PEI are tremendously more expensive than those realized with traditional polymeric commodities (about 150 € $g^{-1}$ for PEI and not more than 30 € $kg^{-1}$ for the more expensive common polymeric commodities).[27] In this view, the permeability results obtained by the developed HAVOH/Zr/rGO assemblies represent an excellent balance between the material costs and performances.

In order to have a better understanding of the effect of zirconium adducts on enhancement of the barrier properties, the theoretical aspect ratio of nanoplatelets opposing to gas permeation has been calculated by adopting the Cussler model.[28] This model correlates the gas permeability of nanocomposites relative to the pristine polymer ($P/P_0$) with the nanoplatelets concentration ($\phi$) and aspect ratio ($\alpha$) as the ratio of the maximum dimension to the thickness. The model has been used under the assumption that the rGO nanoplatelets assemble as monolayers and that their concentration does not change in each deposited layered assembly (see the Supporting Information, Figure S5 and Table S1). This hypothesis is supported by the observation that the coating thickness increases almost linearly with the number of layered assemblies.

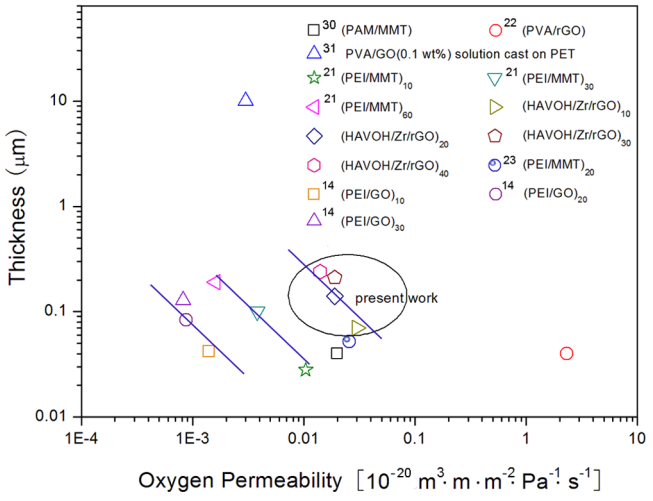


**Figure 4.** Thickness and oxygen permeability of $(HAVOH/Zr/rGO)_n$ multilayered coating assemblies in comparison with those of coatings prepared by other authors by using different technologies (solution-cast and LbL) and different components (polymers/fillers). The numbers shown in the upper right of the panel indicate the references. All data are related to the LbL deposition technique,[14,21−23,30] except one related to solution casting.[31] The coating permeability was decoupled from the total permeability using the method described in the Supporting Information. MMT = montmorillonite; PVA = poly(vinyl alcohol); PEI = polyethylenimine; PAM = polyacrylamide.

The calculated aspect ratio of nanoplatelets increases from 358 to 590 with an increase in the number of layers deposited


DOI: 10.1021/acsami.5b07529
ACS Appl. Mater. Interfaces 2015, 7, 22678−22685

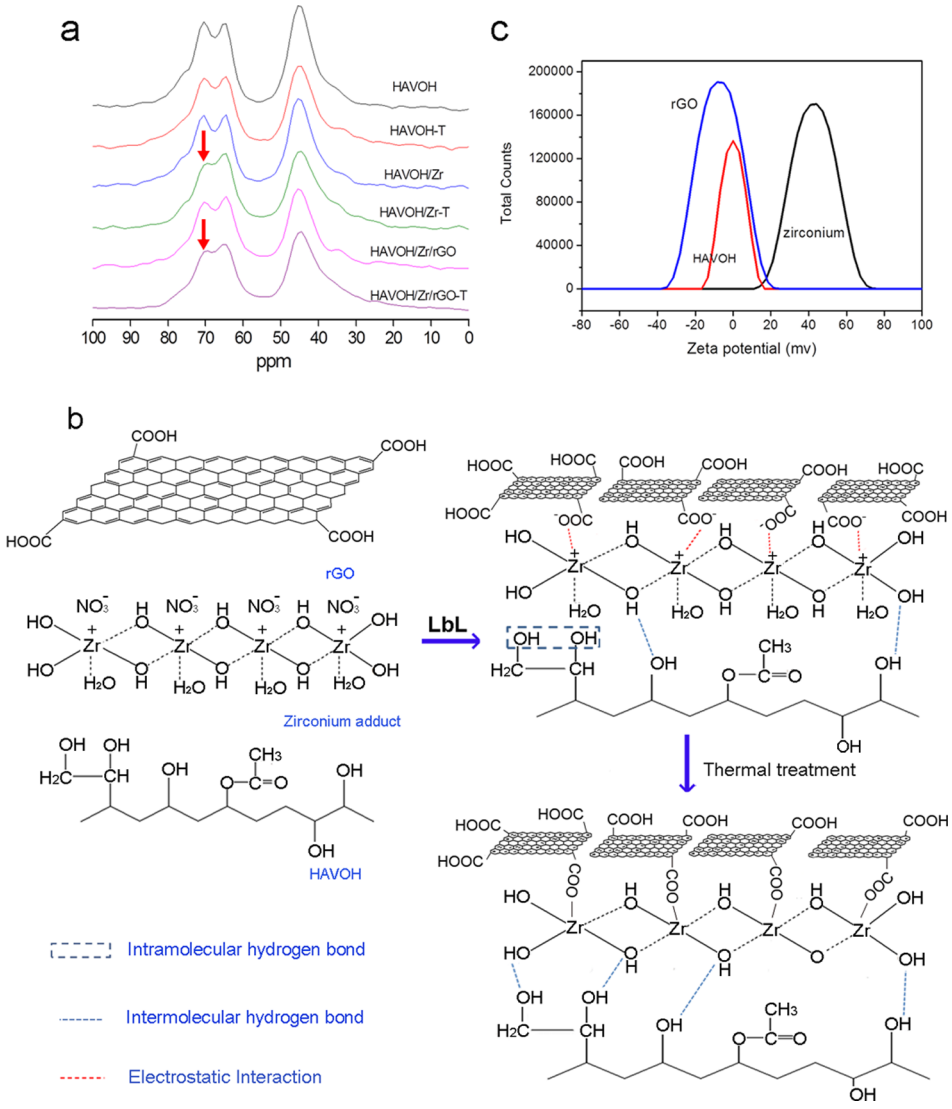


**Figure 5.** (a) $^{13}C$ NMR spectra of HAVOH composite films, (b) schematic representation of the interactions among HAVOH, zirconium adducts, and rGO before and after thermal treatment at 120 °C for 10 min, and (c) $\zeta$ potential of rGO, HAVOH, and zirconium aqueous solutions.

on PET substrates, thus suggesting that the zirconium adducts cross-link the rGO nanoplatelets and contribute to the formation of nanoparticles with increased aspect ratio. This brings about an increment of tortuous pathways for the gas molecules diffusing through the hybrid multilayered coating, with consequent improvement of the barrier properties.

As shown in Figure 3b,c, at 33% and 75% RH conditions, the OTR values of $(HAVOH/Zr/rGO)_n$ coatings increase slightly compared to that at 0% RH. This behavior is attributed to the hydrophilic character of the deposited materials, which absorbs a higher amount of water at high humidity values and thus consequently reduces the barrier properties.

For the sake of comparison, the assemblies obtained by depositing on PET substrate coatings containing a more hydrophilic filler such as GO were also investigated. The OTR decreases with an increase in the number of deposited layers. However, PET coated with GO, i.e., $(HAVOH/Zr/GO)_n$, layers exhibit higher OTR values compared to the sample with rGO, i.e., $(HAVOH/Zr/rGO)_n$, coatings. Also, the $(HAVOH/Zr/GO)_n$ coatings show lower barrier properties when exposed to oxygen fluxes in humid conditions (see the Supporting Information, Figure S6).

In order to further investigate the role of zirconium adducts as chemical cross-linkers, $^{13}C$ NMR measurements of pristine HAVOH and composite films prepared by solution casting, before and after thermal treatment (the samples are designated as T), were performed. In the NMR spectra (Figure 5a), the peak at 46 ppm is assigned to methylene, while the other three peaks corresponding to the methine carbon resonance at 77 (I), 71 (II), and 65 (III) ppm are ascribed to the stereoregular structure of the HAVOH polymer. Peak I (77 ppm) appears as a shoulder on the overall $^{13}C$ NMR profile, indicating the extremely poor stereoregularity of HAVOH. Peak II (71 ppm) in $^{13}C$ NMR spectra for the various HAVOH composite films does not significantly change with the presence of either zirconium or rGO. After thermal treatment, the intensity of peak II at 71 ppm decreases for the HAVOH/Zr and HAVOH/Zr/rGO samples while remaining substantially unchanged for pristine HAVOH. These spectral features indicate that thermal treatment of HAVOH in the presence of zirconium disrupts the intramolecular hydrogen bond formed between the hydroxyl groups in heterotactic (mr) triads and promotes the formation of new interactions between zirconium and the hydroxyl groups of HAVOH, likely via intermolecular hydrogen bonding (see


DOI: 10.1021/acsami.5b07529
ACS Appl. Mater. Interfaces 2015, 7, 22678−22685

Figure 5b). In fact, because of the fact that zirconium oxynitrate exists in aqueous solution as polymeric adducts (i.e., tetrameric units), in which four zirconium atoms are linked by hydroxyl groups, it is expected that hydrogen bonding takes place between the hydroxyl groups present in polymeric zirconium adducts and the hydroxyl groups present in the molecular structure of HAVOH. On the other hand, it has been verified that the zirconium adducts show a positive charge ($\zeta$ potential: 40 mV, as shown in Figure 5c), which allows a strong electrostatic interaction with rGO nanoplatelets ($\zeta$ potential: −10 mV, as shown Figure 5c). Polymeric zirconium adducts can also interact through electrostatic interaction with carboxylate groups commonly located on the edge of rGO. This specific interaction upon thermal treatment may form a metal−organic ester with the formation of a covalent bond.[29] In this view, the zirconium polymeric adducts act as cross-linkers between HAVOH and rGO building blocks, thus promoting the higher rGO surface coverage density previously shown by the AFM results, and also as interlinkers between HAVOH layers deposited through two consecutive cycles. At the same time, as confirmed by determination of the theoretical aspect ratio, the zirconium polymeric adducts contribute to increase the aspect ratio of nanoplatelets through the formation of covalent bonds with rGO nanoplatelets. In Figure 5b is reported a schematic representation of possible interactions taking place between zirconium polymeric adducts and HAVOH polymers and rGO nanoplatelets.

The proposed network brings about a marked increment of the overall tortuosity pathways of the oxygen molecules permeating through the organic−inorganic hybrid coating. The role of zirconium adducts as binders between HAVOH and rGO layers was further validated through nanoindentation measurements. The results show that $(HAVOH/Zr/rGO)_n$ hybrid coatings exhibit a higher resistance to indentation than $(HAVOH/rGO)_n$ coatings, indicating the effect of zirconium adducts to compact HAVOH and rGO layers through the formation of a tight network (Figure S7 in the Supporting Information).

## 3. CONCLUSIONS

In summary, multilayered hybrid coatings consisting of alternate layers of rGO nanosheets and HAVOH with zirconium adducts as binders were successfully fabricated through a LbL assembly approach. AFM analysis showed that rGO nanoplatelets were uniformly dispersed over the HAVOH polymer substrate and that the $(HAVOH/Zr/rGO)_n$ hybrid coatings exhibited higher rGO surface coverage densities than the $(HAVOH/rGO)_n$ coatings. SEM and TEM revealed that multilayer $(HAVOH/Zr/rGO)_n$ hybrid coatings exhibited a brickwall structure with HAVOH and rGO as buildings blocks. A significant improvement in the oxygen barrier properties was achieved for the PET samples coated with $(HAVOH/Zr/rGO)_n$ hybrid coatings compared to pristine PET. In particular, the OTR of the sample coated with 40 three-layer HAVOH/Zr/rGO is decreased by 95% in dry conditions. This is attributed to the effect of zirconium polymeric adducts, which enhance the assembling efficiency of rGO and compact the layers, as confirmed by NMR characterization, resulting in a significant increment of the oxygen-transport pathways. Thanks to the tunable chemistry of zirconium adducts, this work demonstrates that the LbL approach can also be adopted for nonpolar polymers as HAVOH and brings new potential opportunities for organic−inorganic high-barrier LbL coatings in the packaging industry.

## 4. EXPERIMENTAL SECTION

**rGO Fabrication.** GO was synthesized from purified natural graphite according to Hummers' method.[32] The chemical rGO was obtained through a reduction process by using L-ascorbic acid as the reducing agent, according to the previous reports.[33]

**Preparation of HAVOH Composite Films.** HAVOH composite films used for the chemical characterization of zirconium adducts as cross-linkers were produced by the solvent-mixing and -casting approach. In brief, HAVOH polymer (0.2 g) was dissolved in distilled water (20 mL) and stirred for 4 h at 50 °C. Then 20 mL of a zirconium aqueous solution (0.1 wt %) was added to the HAVOH solution; the mixture was stirred for 1 h to get a homogeneous HAVOH/Zr solution. A total of 20 mL of a rGO aqueous dispersion (0.1 mg $mL^{-1}$) was added dropwise to the above solution, and the resulting mixture was stirred for 1 h at room temperature and then sonicated for 30 min in an ultrasonic bath. The obtained dispersion was then poured into a Petri plastic dish and dried in a fume hood until the water was completely evaporated. For thermal treatment, the cast films were put into a vacuum oven at 120 °C for 10 min.

**LbL Coatings Fabrication on Silicon and Quartz Substrates.** The LbL coatings deposited on silicon and quartz substrates and used for the morphological characterization of the coatings were prepared through a preliminary activation procedure of the surfaces. In detail, single side-polished silicon wafers were treated by piranha treatment with a 1:3 ratio of hydrogen peroxide (30% v/v) to sulfuric acid (99 wt %) and stored in deionized water before being used as the substrate for deposition of the coating before AFM measurement. Quartz slides were cleaned with acetone and deionized water and used as substrates for UV−vis absorption analysis of the deposited coatings.

**Characterization.** The UV−vis absorption spectra of a GO and rGO aqueous dispersion were measured on a Lambda 35 (PerkinElmer) spectrophotometer. The stepwise buildup of $(HAVOH/Zr/rGO)_n$ coatings with $n$ = 1, 2, ..., 10 assemblies deposited on quartz substrates was monitored through UV−vis absorption spectra collected with a Jasco V-570 spectrometer in the 200−800 nm wavelength range.

Cross sections of the $(HAVOH/Zr/rGO)_n$ hybrid coatings were imaged with a FEI Fecnai G2 F20 S-Twin transmission electron microscope, operating at an accelerating voltage of 200 kV. The film was embedded in an epoxy resin, supporting the LbL coatings prior to sectioning with a microtome.

Scanning electron microscopy (SEM) observation was performed using an Inspect F model FEI apparatus at an accelerating voltage of 10 kV. The samples with the multilayered coatings were fractured in liquid nitrogen and then sputter-coated with gold.

AFM analysis was carried out at room temperature (25 °C) by using a silicon cantilever (Bruker Corp., Santa Barbara, CA) with a rotated tip of a nominal radius of 8 nm. The scan rate was 0.2 Hz, while the scan area was 10 × 10 $\mu m^2$. All data were processed (first-order planefit) during the AFM raster.

The oxygen transmission rate (OTR) was evaluated by using a standard permeabilimeter (Extrasolution, MULTIPERM) at 23 °C and 0%, 33%, and 75% RH.

A 300 MHz Bruker AVANCE magnet, equipped with a 4 mm wide-bore magic-angle-spinning probe (operating at the $^{13}C$ frequency of 75.4 MHz), was used to collect $^{13}C$ NMR spectra by a cross-polarization magic-angle-spinning technique. Each sample (70−90 mg) was packed in 4 mm zirconia rotors with Kel-F caps prior to being loaded into the magnet and spun at a rate of 13000 ± 1 Hz. All spectra have been processed and elaborated by Bruker *Topspin* software, version 2.1 (Bruker Biospin, Rheinstetten, Germany).

The $\zeta$ potential of the rGO, HAVOH, and zirconium aqueous suspension was measured by dynamic light scattering (Zetasizer Nano ZS90, Malvern, U.K.).


DOI: 10.1021/acsami.5b07529
ACS Appl. Mater. Interfaces 2015, 7, 22678−22685

## ■ ASSOCIATED CONTENT

### Supporting Information

The Supporting Information is available free of charge on the ACS Publications website at DOI: 10.1021/acsami.5b07529.

Detailed experimental materials and methods, UV−vis absorption spectra, Raman spectra, XPS results, oxygen permeability, Gi-SAXS, Cussler model, and nanoindentation results (PDF)

## ■ AUTHOR INFORMATION


### Corresponding Authors

*E-mail: mlavorgn@unina.it.
*E-mail: xiahs@scu.edu.cn.


### Author Contributions

The manuscript was written through contributions of all authors. All authors have given approval to the final version of the manuscript.

### Notes

The authors declare no competing financial interest.

## ■ ACKNOWLEDGMENTS

This work has been carried out in the framework of both the International Multifunctional Polymers and Biomaterials, MPB Research Center, established between the Department of Chemical Science and Materials Technology of the National Research Council (Italy) and Sichuan University (China) and the Joint Laboratory for Graphene-based Multifunctional Polymer Nanocomposites supported by CNR (Project 2710 IPCB-CNR). This work is supported also by International Science & Technology Cooperation Program of China (Grant 2015DFA51110). Finally, financial support from the program PON Ricerca e Competitività 2007−2013, cofinanced by the European Regional Development Fund, within the Research Project PON01 00636 FINGERIMBALL is also gratefully acknowledged. The authors acknowledge Alessandra Aldi for her technical support in the preparation and characterization of the materials and Enza Migliore for support in the preparation of drawings and graphical schemes.

## ■ REFERENCES


(1) Balandin, A. A.; Ghosh, S.; Bao, W. Z.; Calizo, I.; Teweldebrhan, D.; Miao, F.; Lau, C. N. Superior Thermal Conductivity of Single Layer Graphene. *Nano Lett.* **2008**, *8*, 902−907.

(2) Novoselov, K. S.; Geim, A. K.; Morozov, S. V.; Jiang, D.; Katsnelson, M. I.; Grigorieva, I. V.; Dubonos, S. V.; Firsov, A. A. Two-Dimensional Gas of Massless Dirac Fermions in Graphene. *Nature* **2005**, *438*, 197−200.

(3) Stankovich, S.; Dikin, D. A.; Dommett, G. H. B.; Kohlhaas, K. M.; Zimney, E. J.; Stach, E. A.; Piner, R. D.; Nguyen, S. T.; Ruoff, R. S. Graphene Based Composite Materials. *Nature* **2006**, *442*, 282−286.

(4) Lee, C.; Wei, X. D.; Kysar, J. W.; Hone, J. Measurement of the Elastic Properties and Intrinsic Strength of Monolayer Graphene. *Science* **2008**, *321*, 385−388.

(5) Su, Y.; Kravets, V. G.; Wong, S. L.; Waters, J.; Geim, A. K.; Nair, R. R. Impermeable Barrier Films and Protective Coatings Based on Reduced Graphene Oxide. *Nat. Commun.* **2014**, *5*, 4843.

(6) Yoo, B. M.; Shin, H. J.; Yoon, H. W.; Park, H. B. Graphene and Graphene Oxide and Their Uses in Barrier Polymers. *J. Appl. Polym. Sci.* **2014**, *131*, 39628−39650.

(7) Bunch, J. S.; Verbridge, S. S.; Alden, J. S.; van der Zande, A. M.; Parpia, J. M.; Craighead, H. G.; McEuen, P. L. Impermeable Atomic Membranes from Graphene Sheets. *Nano Lett.* **2008**, *8*, 2458−2462.

(8) Scherillo, G.; Lavorgna, M.; Buonocore, G. G.; Zhan, Y. H.; Xia, H. S.; Mensitieri, G.; Ambrosio, L. Tailoring Assembly of Reduced Graphene Oxide Nanosheets to Control Gas Barrier Properties of Natural Rubber Nanocomposites. *ACS Appl. Mater. Interfaces* **2014**, *6*, 2230−2234.

(9) Zhan, Y. H.; Lavorgna, M.; Buonocore, G.; Xia, H. S. Enhancing Electrical Conductivity of Rubber Composites by Constructinginterconnected Network of Self-Assembled Graphene with Latex Mixing. *J. Mater. Chem.* **2012**, *22*, 10464−10468.

(10) Guadagno, L.; Raimondo, M.; Vertuccio, L.; Mauro, M.; Guerra, G.; Lafdi, K.; De Vivo, B.; Lamberti, P.; Spinelli, G.; Tucci, V. Optimization of Graphene Based Materials Outperforming Host Epoxy Matrices. *RSC Adv.* **2015**, *5*, 36969−36978.

(11) Bao, C. L.; Guo, Y. Q.; Song, L.; Hu, Y. Poly(Vinyl Alcohol) Nanocomposites Based on Graphene and Graphite Oxide: A Comparative Investigation of Property and Mechanism. *J. Mater. Chem.* **2011**, *21*, 13942−13950.

(12) Kim, F.; Cote, L. J.; Huang, J. Graphene Oxide: Surface Activity and Two-Dimensional Assembly. *Adv. Mater.* **2010**, *22*, 1954−1958.

(13) Putz, K. W.; Compton, O. C.; Palmeri, M. J.; Nguyen, S. T.; Brinson, L. C. High-Nanofiller-Content Graphene Oxide-Polymer Nanocomposites via Vacuum- Assisted Self-Assembly. *Adv. Funct. Mater.* **2010**, *20*, 3322−3329.

(14) Yang, Y. H.; Bolling, L.; Priolo, M. A.; Grunlan, J. C. Super Gas Barrier and Selectivity of Graphene Oxide-Polymer Multilayer Thin Films. *Adv. Mater.* **2013**, *25*, 503−508.

(15) Chen, J. T.; Fu, Y. J.; An, Q. F.; Lo, S. C.; Huang, S. H.; Hung, W.-S.; Hu, C.-C.; Lee, K.-R.; Lai, J.-Y. Tuning Nanostructure of Graphene Oxide/Polyelectrolyte LbL Assemblies by Controlling pH of GO Suspension To Fabricate Transparent and Super Gas Barrier Film. *Nanoscale* **2013**, *5*, 9081−9088.

(16) Chen, D.; Wang, X. Y.; Liu, T. X.; Wang, X. D.; Li, J. Electrically Conductive Poly (Vinyl Alcohol) Hybrid Films Containing Graphene and Layered Double Hydroxide Fabricated via Layer-By-Layer Self-Assembly. *ACS Appl. Mater. Interfaces* **2010**, *2*, 2005−2011.

(17) Sham, A. Y. W.; Notley, S. M. Layer-by-Layer Assembly of Thin Films Containing Exfoliated Pristine Graphene Nanosheets and Polyethyleneimine. *Langmuir* **2014**, *30*, 2410−2418.

(18) Such, G. K.; Quinn, J. F.; Quinn, A.; Tjipto, E.; Caruso, F. Assembly of Ultrathin Polymer Multilayer Films by Click Chemistry. *J. Am. Chem. Soc.* **2006**, *128*, 9318−9319.

(19) Buck, M. E.; Zhang, J.; Lynn, D. M. Layer-by-Layer Assembly of Reactive Ultrathin Films Mediated by Click-Type Reactions of Poly (2-Alkenyl Azlactone)s. *Adv. Mater.* **2007**, *19*, 3951−3955.

(20) Zhao, X.; Zhang, Q. H.; Hao, Y. Q.; Li, Y. Z.; Fang, Y.; Chen, D. J. Alternate Multilayer Films of Poly(vinyl alcohol) and Exfoliated Graphene Oxide Fabricated via a Facial Layer-by-Layer Assembly. *Macromolecules* **2010**, *43*, 9411−9416.

(21) Priolo, M. A.; Gamboa, D.; Grunlan, J. C. Transparent Clay-Polymer Nano Brick Wall Assemblies with Tailorable Oxygen Barrier. *ACS Appl. Mater. Interfaces* **2010**, *2*, 312−320.

(22) Yu, L.; Lim, Y. S.; Han, J. H.; Kim, K. Y.; Kim, J. Y.; Choi, S. Y.; Shin, K. A Graphene Oxide Oxygen Barrier Film Deposited via a Self-Assembly Coating Method. *Synth. Met.* **2012**, *162*, 710−714.

(23) Priolo, M. A.; Holder, K. M.; Gamboa, D.; Grunlan, J. C. Influence of Clay Concentration on the Gas Barrier of Clay Polymer Nanobrick Wall Thin Film Assemblies. *Langmuir* **2011**, *27*, 12106−12114.

(24) Byrd, H.; Whipps, S.; Pike, J. K.; Ma, J. F.; Nagler, S. E.; Talham, D. R. Role of the Template Layer in Organizing Self-Assembled Films: Zirconium Phosphonate Monolayers and Multilayers at a Langmuir-Blodgett Template. *J. Am. Chem. Soc.* **1994**, *116*, 295−301.

(25) Keller, S. W.; Kim, H. N.; Mallouk, T. E. Layer-by-Layer Assembly of Intercalation Compounds and Heterostructures on Surfaces: Toward Molecular "Beaker" Epitaxy. *J. Am. Chem. Soc.* **1994**, *116*, 8817−8818.

(26) Putvinski, T. M.; Schilling, M. L.; Katz, H. E.; Chidsey, C. E. D.; Mujsce, A. M.; Emerson, A. B. Self -Assembly of Organic Multilayers




DOI: 10.1021/acsami.5b07529
*ACS Appl. Mater. Interfaces* 2015, 7, 22678−22685

with Polar Order Using Zirconium Phosphate Bonding between Layers. *Langmuir* **1990**, *6*, 1567−1571.
(27) www.sigmaaldrich.com/catalog/search.
(28) Wong, M. H.; Ishige, R.; White, K. L.; Li, P.; Kim, D.; Krishnamoorti, R.; Gunther, R.; Higuchi, T.; Jinnai, H.; Takahara, A.; Nishimura, R.; Sue, H. J. Large-scale Self-assembled Zirconium Phosphate Smectic Layers via a Simple Spray-coating Process. *Nat. Commun.* **2014**, DOI: 10.1038/ncomms4589.
(29) Spring, J. L. B.; Tomball, A. S. M.; Spring, J. C. D. U.S. Patent 5,497,830, 1996.
(30) Jang, W. S.; Rawson, I.; Grunlan, J. C. Layer-by-layer Assembly of Thin Film Oxygen Barrier. *Thin Solid Films* **2008**, *516*, 4819−4825.
(31) Lai, C. L.; Chen, J. T.; Fu, Y. J.; Liu, W. R.; Zhong, Y. R.; Huang, S. H.; Hung, W. S.; Lue, S. J.; Hu, C. C.; Lee, K. R. Bio-Inspired Cross-Linking with Borate for Enhancing Gas-Barrier Properties of Poly(Vinyl Alcohol)/Graphene Oxide Composite Film. *Carbon* **2015**, *82*, 513−522.
(32) Hummers, W. S.; Offeman, R. E. Preparation of Graphitic Oxide. *J. Am. Chem. Soc.* **1958**, *80*, 1339−1339.
(33) Fernández-Merino, M. J. F.; Guardia, L.; Paredes, J. I.; Villar-Rodil, S.; Solis-Fernández, P.; Martínez-Alonso, A.; Tascón, J. M. D. Vitamin C Is an Ideal Substitute for Hydrazine in the Reduction of Graphene Oxide Suspensions. *J. Phys. Chem. C* **2010**, *114*, 6426−6432.


DOI: 10.1021/acsami.5b07529
*ACS Appl. Mater. Interfaces* 2015, 7, 22678−22685